

The Charge Transfer Problem in Density Functional Theory Calculations of Aqueously Solvated Molecules

Christine M. Isborn,^{*†} Brendan D. Mar,^{‡,§} Basile F. E. Curchod,^{||} Ivano Tavernelli,^{||} and Todd J. Martínez^{‡,§}

[†]Chemistry and Chemical Biology, University of California Merced, Merced, California 95343, United States

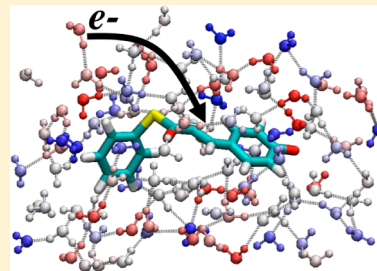
[‡]PULSE Institute and Department of Chemistry, Stanford University, Stanford, California 94305, United States

[§]SLAC National Accelerator Laboratory, Menlo Park, California 94025, United States

^{||}Laboratory of Computational Chemistry and Biochemistry, Ecole Polytechnique Fédérale de Lausanne, CH-1015 Lausanne, Switzerland

Supporting Information

ABSTRACT: Recent advances in algorithms and computational hardware have enabled the calculation of excited states with time-dependent density functional theory (TDDFT) for large systems of $O(1000)$ atoms. Unfortunately, the aqueous charge transfer problem in TDDFT (whereby many spuriously low-lying charge transfer excited states are predicted) seems to become more severe as the system size is increased. In this work, we concentrate on the common case where a chromophore is embedded in aqueous solvent. We examine the role of exchange-correlation functionals, basis set effects, ground state geometries, and the treatment of the external environment in order to assess the root cause of this problem. We conclude that the problem rests largely on water molecules at the boundary of a finite cluster model, i.e., “edge waters.” We also demonstrate how the TDDFT problem can be related directly to ground state problems. These findings demand caution in the commonly employed strategy that rests on “snapshot” cutout geometries taken from ground state dynamics with molecular mechanics. We also find that the problem is largely ameliorated when the range-separated hybrid functional LC- ω PBEh is used.



1. INTRODUCTION

Because many experiments are on solvated molecules and solvation is ubiquitous in biological systems, accurate modeling of solvation is very desirable. Recent advances in both algorithms and computer hardware have made fully quantum mechanical (QM) calculations tractable for $O(1000)$ atoms,^{1–6} enabling explicit QM modeling of both ground^{7,8} and excited^{9,10} electronic states in solvated systems. However, such QM modeling of solvation remains challenging both because of the high cost of large QM calculations and because of the need to sample many solvent configurations. Modeling solvent configurations with molecular mechanics (MM) methods has a much smaller computational cost, but this technique cannot model charge transfer or hydrogen atom/proton transfer, and fixed charge models cannot describe polarization of the solvent. Continuum models remove explicit solute–solvent interactions in favor of a polarizable dielectric surrounding the solute.^{11,12} In addition to including polarization, these continuum models have the added benefit of removing the need for sampling over many solvent configurations. While modeling solvation with explicit QM waters is the most computationally intensive of these methods, it is also the only method that includes explicit solvent interactions that take into account charge-transfer and polar-

ization, and thus should be the most accurate solvation technique given a large enough solvation shell.

One possible approach to quantum mechanical modeling of solvation is via a ‘droplet’ method, in which a shell of solvent molecules is included in the calculation. This can lead to artificial edge effects from the solvent shell being exposed to vacuum. Additionally, if the absorption spectrum is desired via excited state calculations, it is known that the QM excited state methodology workhorse, time-dependent density functional theory, TDDFT,¹³ spuriously places charge-transfer (CT) states too low in energy when standard functionals are employed.^{14–16} For aqueous solvation the problem is particularly egregious, with local or generalized gradient approximation (GGA) functionals giving many low-energy dark CT states below the bright valence states of the solute that are of interest.^{17–20} With many low-lying dark states in solvated systems, the standard Davidson procedure of solving for the lowest lying excited states becomes very computationally intensive (for both memory and time), as more and more states must be solved for in order to reach the valence transitions of spectroscopic interest. Thus, not only are the

Received: June 12, 2013

Revised: August 12, 2013

Published: August 21, 2013

predictions incorrect, they are computationally costly. Furthermore, the presence of spurious low-lying states renders any simulation of excited state dynamics impossible or at least ill-advised. In this work, we examine the CT problem for solvated chromophores from both the ground state (DFT) and excited state (TDDFT) perspective.

2. THEORY

As demonstrated previously,^{14,16} the poor description of CT excited states in TDDFT can be traced back to the lack of Coulombic attraction between the excited electron (e^-) and the hole (h^+) it leaves behind (i.e., bound excitons). One might expect this to be modeled with the classical Coulomb (i.e., Hartree) functional $J[\rho]$. However, this is not the case, and instead the exchange-correlation functional $K_{xc}[\rho]$ is tasked with describing this electron–hole interaction in TDDFT. Local and semilocal approximations to K_{xc} completely neglect the e^-h^+ Coulomb attraction, while fully nonlocal Hartree–Fock (HF) exchange includes the proper $1/r$ Coulombic attraction between the electron and hole.

Within the adiabatic approximation, the matrix equations for the linear response formalism of TDDFT and time-dependent Hartree–Fock (TDHF) are

$$\begin{pmatrix} \mathbf{A} & \mathbf{B} \\ \mathbf{B} & \mathbf{A} \end{pmatrix} \begin{pmatrix} \mathbf{X} \\ \mathbf{Y} \end{pmatrix} = \omega \begin{pmatrix} 1 & 0 \\ 0 & -1 \end{pmatrix} \begin{pmatrix} \mathbf{X} \\ \mathbf{Y} \end{pmatrix} \quad (1)$$

where ω are the excitation energies from the ground state density, \mathbf{X} and \mathbf{Y} represent the transition densities between the ground and excited states, and the \mathbf{A} and \mathbf{B} matrices describe the linear response of the ground state density matrix to a perturbation. For TDHF (ignoring spin for simplicity), these matrices are given by

$$\mathbf{A}_{ai,bj} = \delta_{ij}\delta_{ab}(\epsilon_a - \epsilon_i) + (ialbj) - (ijlab) \quad (2)$$

$$\mathbf{B}_{ai,bj} = (ialbj) - (iblaj) \quad (3)$$

$$(ialbj) = \int \int \frac{\phi_i(\mathbf{r}_1)\phi_a(\mathbf{r}_1)\phi_j(\mathbf{r}_2)\phi_b(\mathbf{r}_2)}{|\mathbf{r}_1 - \mathbf{r}_2|} d\mathbf{r}_1 d\mathbf{r}_2 \quad (4)$$

where ϵ_a and ϵ_i are the unoccupied and occupied HF molecular orbital (MO) eigenvalues, respectively. For TDDFT the comparable linear response equations are²¹

$$\mathbf{A}_{ai,bj} = \delta_{ij}\delta_{ab}(\epsilon_a - \epsilon_i) + (ialbj) + (ialf_{xc}|jb) \quad (5)$$

$$\mathbf{B}_{ai,bj} = (ialbj) + (ialf_{xc}|bj) \quad (6)$$

$$(ialf_{xc}|jb) = \int \int \phi_i(\mathbf{r}_1)\phi_a(\mathbf{r}_1) \frac{\delta^2 E_{xc}}{\delta \rho(\mathbf{r}_1)\delta \rho(\mathbf{r}_2)} \phi_j(\mathbf{r}_2)\phi_b(\mathbf{r}_2) d\mathbf{r}_1 d\mathbf{r}_2 \quad (7)$$

in which ϵ_a and ϵ_i are now the unoccupied and occupied Kohn–Sham (KS) MO eigenvalues, the exchange-like term resulting from the Coulomb interaction of the electrons remains the same, and the Coulomb-like term resulting from the exchange interaction of the electrons is replaced by the second derivative of the exchange-correlation energy with respect to the electron density. Within the CIS approximation for TDHF and the corresponding Tamm-Danoff approximation (TDA) for TDDFT, the \mathbf{B} matrix is neglected and only the leading \mathbf{A} matrix remains:

$$\mathbf{AX} = \omega \mathbf{X} \quad (8)$$

The diagonal elements of \mathbf{A} , where $i = j$ and $a = b$, correspond to energies for an excited electron and hole. In CIS, the final term in eq 2 yields the proper Coulombic attraction of the electron and hole, resulting in the correct (for CT states) $1/r$ energy dependence on distance r between electron donor and acceptor. This term stems from the exact exchange in the HF energy, which is missing from approximate nonhybrid density functionals. As a result, TDDFT calculations with local or generalized gradient approximation (GGA) functionals predict qualitatively incorrect e^-h^+ distance dependence for CT state energies. Hybrid functionals, which include some fraction of HF exchange, mitigate the CT problem of TDDFT by restoring the e^-h^+ Coulombic attraction for CT states (although the expected $1/r$ behavior is recovered only when the exact exchange contribution is unscaled).

Range-separated hybrid density functionals go beyond simple hybrids to include complete HF exact exchange at long-range.²² This class of density functionals shows substantial improvement in the treatment of CT electronic excitations.^{23,24} For these long-range corrected (LC) functionals the Coulomb operator $1/r$ is separated into short-range and long-range components. Because of the ease of integral computation when using Gaussian atomic orbitals, this separation is generally accomplished using a smoothly varying error function:

$$\frac{1}{r_{ij}} \equiv \frac{\text{erf}(\mu r_{ij})}{r_{ij}} + \frac{\text{erfc}(\mu r_{ij})}{r_{ij}} \quad (9)$$

in which μ (often also denoted γ or ω , which could cause some confusion with ω representing the excitation energies) is a parameter that determines the interelectronic distance for crossing over between short- and long-range exchange. The μ parameter is generally determined empirically, but recent work shows that improved results can be obtained by tuning μ for the system or molecule or geometry of interest.^{25–28}

In LC density functionals, the exact exchange contribution to the energy is given by

$$E_x^{lr-EX} = -\frac{1}{2} \sum_{ij}^{nocc} \int \int \phi_i(\mathbf{r}_1)\phi_j(\mathbf{r}_1) \frac{\text{erf}(\mu r_{12})}{|\mathbf{r}_1 - \mathbf{r}_2|} \phi_i(\mathbf{r}_2)\phi_j(\mathbf{r}_2) d\mathbf{r}_1 d\mathbf{r}_2 \quad (10)$$

The total LC DFT energy is then determined by the standard DFT exchange energy at short range, HF exchange energy at long range, a mix of the two kinds of exchange at midrange, and the DFT correlation energy at all interelectronic distances:

$$E_{xc}^{\text{LC-DFT}}[\rho] = E_x^{\text{DFT}}[\rho] + (E_x^{lr-EX}[\rho] - E_x^{lr-DFT}[\rho]) + E_c^{\text{DFT}}[\rho] \quad (11)$$

The inclusion of HF exchange at long range is found to raise the energy of CT states and to restore the expected $1/r$ dependence of CT state energies. However, full inclusion of exchange at both short and long range without electron correlation, as in the CIS method, reverses the problem and places CT transitions too high in energy. The electron correlation energy (neglected by CIS) is expected to be larger for CT states where part of the molecule is negatively charged. This leads to a systematic bias toward overly large excitation energies for CT states, as has been recently demonstrated.²⁹ Thus, exact exchange serves to restore the proper asymptotic behavior for CT states.

Because modeling solvation with many QM waters poses an extreme CT problem for standard TDDFT, we wanted to know how hybrid and LC-TDDFT would fare in this situation. In particular, would the good CT behavior of LC-TDDFT break down and also have a CT problem when many (more than 100) QM waters were included in the excited state computation? Work by Herbert and co-workers²⁰ has shown that the simple technique of including a point charge electrostatic environment around the QM water droplet decreases the number of spurious low-energy CT states. The origin of this improvement is unclear. We herein examine why and how well this technique works for reducing the CT problem, along with other simple techniques to reduce spurious low-energy CT states computed with TDDFT when a solute is solvated with QM waters.

We use two standard chromophoric molecules for our studies here: the anionic chromophore of photoactive yellow protein (PYP) *trans*-thiophenyl-*p*-coumarate (pCT^-)^{30–32} and the commonly used solvatochromic probe and laser dye Nile Red,^{33–35} both shown in Figure 1. Description of the excited

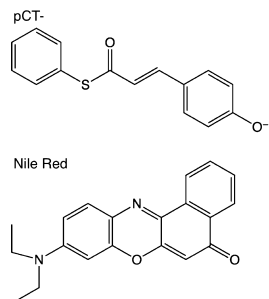


Figure 1. Structures of *trans*-thiophenyl-*p*-coumarate (pCT^-) and Nile Red.

states of the PYP chromophore in vacuum has proven quite challenging.^{36–39} Recent work suggests that for a model PYP chromophore similar to pCT^- a multireference method that includes double and triple excitations is necessary to obtain a computed excited state energy that agrees with the vacuum experimental value.^{40,41} This previous work calculated the TD-CAM-B3LYP/aug-cc-pVDZ bright transition in vacuum to be 0.4–0.6 eV too high in energy compared to post-SCF methods and experiment.⁴² For pCT^- a large solvatochromic blue-shift of 0.44 eV was measured experimentally in going from vacuum to aqueous buffer solution, with an aqueous absorption maxima at 395 nm (3.14 eV).⁴² In contrast, TDDFT predicts a red shift, irrespective of whether the solvent is modeled using explicit QM waters⁹ or a dielectric continuum.⁴³

While the ground state of anionic charge-separated pCT^- is preferentially stabilized over the excited state in polar solvent causing the blue-shift, neutral Nile Red undergoes a red-shift with increasing solvent polarity, indicating a larger dipole moment in the excited state than in the ground state.^{33–35} For Nile Red, the red-shift in λ_{max} going from solvation in pentane to water is ~0.5 eV, with an aqueous absorption maximum of 593 nm (2.09 eV).³⁴ TDDFT with a polarizable continuum method has done well at modeling this red shift for a small range of dielectric constants, capturing the ~0.06 eV red shift in going from benzene to acetonitrile.⁴⁴

In this work we study the problem of aqueous solvation by DFT and TDDFT. We showcase the problem at both the ground state DFT and excited state TDDFT levels, comparing

GGA functionals, LC functionals, and a hybrid functional, along with HF and CIS. We then explore the basis set dependence of the problem and also show how the geometry of the waters around a solute affects the energy levels of the CT states. Finally, we analyze the effects of surrounding the solvating QM waters with MM water point charges and with a polarizable continuum model, and the effects of periodic boundary conditions.

3. COMPUTATIONAL DETAILS

Within a classical Franck–Condon approximation, the electronic absorption spectrum for the $S_0 \rightarrow S_1$ transition in an isotropic system may be modeled as⁴⁵

$$S_{S1}(\omega) \propto \left\{ \int P(R) \delta(\omega - \hbar^{-1}[E_{S1}(R) - E_{S0}(R)]) \right. \\ \times \left. \|\vec{\mu}^{S0/S1}(R)\|^2 dR \right\} / \left[\int P(R) dR \right] \quad (12)$$

where ω is the photon frequency, R denotes the coordinates of the nuclei, $P(R)$ is the probability distribution on the S_0 electronic state, $\vec{\mu}^{S0/S1}(R)$ is the transition dipole moment vector, and $E_{S0}(R)$ is the potential energy on S_0 for molecular coordinates R . This can be straightforwardly extended to include multiple electronic excited states. It is often convenient to replace $P(R)$ with $P^{\text{MM}}(R)$, i.e., to sample molecular configurations on the ground state using a molecular mechanics Hamiltonian. Furthermore, since electronic excitation is often quite localized to a chromophore, it is common to calculate the electronic energy gap, $E_{S1}(R) - E_{S0}(R)$, using a subset of the total system. For example, for a hydrated chromophore, one might choose this subset to be the chromophore and all water molecules within a cutoff radius. This procedure is often used in conjunction with sampling of the ground state probability distribution using periodic boundary conditions.^{9,18,20,46} It should be recognized that the classical approximation implicit in eq 12 implies that vibrational progressions will not be properly modeled. Nevertheless, this approach should provide an adequate accounting of the broad features of the absorption spectrum.

In the present work, our primary interest is not in any particular absorption spectrum, but rather to understand the limitations of TDDFT. Thus, we focus on a single snapshot/geometry from the ground state sampling and do not average to produce a full absorption spectrum as in eq 12. The results shown are representative of what would be seen for other sampled geometries. We perform molecular dynamics with a large periodic water box, then take a snapshot at a single point in time. For this work we carve out increasingly larger droplets of water around the solute. These snapshot substructures are then used as input for the TDDFT excited state calculation. The geometries of pCT^- and Nile Red studied in this work are obtained from a single snapshot of MM dynamics using the Generalized AMBER force field (GAFF) as implemented within the AMBER software package⁴⁷ and the TIP3P MM water model.⁴⁸ Results could be significantly different when using geometries from QM dynamics, but this comparison is beyond the scope of the current work.

Our studies in sections 4.1–4.3 include the closest water molecules to the chromophore for the chosen MM dynamics snapshot. In section 4.4 we explore the effects of relaxing the water shell geometry. We start with the same snapshot subset water/chromophore geometry, but then optimize the locations

and orientations of the water molecules using the MM force field, fixing the chromophore coordinates. The coordinates of all structures are given in the Supporting Information.

The MM dynamics and optimization procedure are as follows. The TIP3P water model⁴⁸ is used with a periodic water box containing 1597 water molecules for pCT⁻ and 3214 waters for Nile Red. After 1000 steps of unconstrained minimization, 500 steps of minimization are performed using SHAKE to constrain hydrogen bonds. Then, NVT equilibration dynamics are run for 10 ps at 300 K, followed by 200 ps of NPT dynamics at 300 K. After 1 ps of NVT production Langevin dynamics at 300 K with a collision frequency of 5 ps⁻¹, a snapshot is taken and the closest waters are carved out at various distances from the solute center. For the water relaxation in section 4.4, the water geometries for the droplet are relaxed (constraining the chromophore geometry) for at least 5000 steps of steepest descent (until the energy lowering between successive steps was at most 0.01 kcal/mol).

In this work we compare the ground and excited state aqueous charge-transfer behavior with the following density functional methods: local gradient corrected GGA functionals BLYP^{49,50} and PBE,⁵¹ the popular semiempirical hybrid B3LYP⁵² which includes 20% HF exchange, the LC version of PBE, and the corresponding hybrid version which includes an additional 20% HF exchange in the short-range component. These last two functionals are denoted as LC- ω PBE^{23,53,54} and LC- ω PBEh,²⁴ respectively, with a range separation parameter of $\mu = 0.2 \text{ au}^{-1}$. HF and CIS results are also included for comparison. Most of the calculations presented here use the 6-31G basis set. However, we also use the 6-31++G* basis set to explore the role of basis set effects in section 4.3.

We present several figures of the density of states for our ground state calculations. In these figures the number of orbitals in energy intervals of 0.01 au (0.27 eV) is plotted with no smoothing function. For each orbital we determine the contribution for each atom based on the product of the square of the molecular orbital coefficient matrix C and the overlap matrix S: $C \times C^t \times S$. The atomic contributions are then grouped into one of the following components of the system: chromophore, inner waters of the solvation cluster that are closest to the chromophore, or outer waters of the solvation cluster.

The ground state and the corresponding excited state CIS and TDDFT calculations are performed with the TeraChem GPU/CPU based electronic structure package,⁵⁵ using the Tamm-Dancoff approximation to TDDFT.⁵⁶ Calculations using a polarizable continuum model^{57,58} are performed with the GAMESS quantum chemistry software package version 11 Aug 2011 (R1).⁵⁹

We have also carried out plane wave basis set calculations with periodic boundary conditions, both to further examine the role of finite basis set effects and to explore the role of edge effects associated with finite cluster models. Three different systems are examined in this way. The first model, and the one closest to the above solvation cluster method, concerns the pCT•(H₂O)₁₀₁ cluster surrounded by vacuum, using a large 47 × 40 × 39 Å³ box to avoid strong interactions between PBC replicas. The second PBC model is more traditional and removes edge effects by classically equilibrating 385 TIP3P waters surrounding the chromophore, keeping the chromophore atoms restrained at their original geometry. This equilibration is first performed in the NVT ensemble for 1 ns at 300 K and then further equilibrated for 2 ns in the NPT

ensemble at the same temperature. The third model uses this same PBC box as a starting point, but creates a 'bubble' defect by removing 2, 5, or 10 water molecules from different parts of the solvation box close to the edge. The vacancy is created (with the exception of one case, see Table 2) by means of a distance criteria from selected water molecules (see Table 2 and Supporting Information (SI)). The last two systems use an orthorhombic box of dimensions 26.57 × 20.89 × 20.92 Å³. For all three of these models, PBC TD-BLYP calculations are performed using the CPMD software package (v 3.13)⁶⁰ with a plane wave basis set with a cutoff of 90 Ry (believed to be close to the basis set limit). Core electrons are replaced by norm-conserving Martins-Troullier pseudopotentials⁶¹ and a neutralizing positive background charge is added in the Ewald sum calculation of the periodic electrostatic interaction.

4. RESULTS AND DISCUSSION

4.1. The Effect of Aqueous Solvation on the Excitation Energies.

One of the goals of this work is to determine which, if any, DFT methods might be suitable for performing ground and excited state Born–Oppenheimer dynamics of chromophores in solution, particularly in solution involving a large number of explicit QM water molecules. To be suitable for single surface excited state dynamics, the chromophore→chromophore state(s) of interest should be energetically separated from the water→chromophore and chromophore→water CT transitions, while for ground state dynamics, the self-consistent field (SCF) procedure should converge to the correct ground state.

Previous work indicates that local and GGA functionals place excited state CT transitions too low in energy and LC functionals show improved behavior. We want to understand the extent of both the CT problem and the improvement as a function of the number of QM waters. We use two measures of problematic CT behavior in the excited state: sharply decreasing lowest excitation energy and a large increase in the number of low energy states. If the value of the lowest excitation energy remains stable after any solvatochromic shift, and retains chromophore→chromophore character, then spuriously low-energy CT states from the waters are not impinging on the chromophore valence transition of interest. A large number of low energy states below the chromophore valence transition is our other indicator of low energy water→chromophore CT states.

The S₀→S₁ excitation energies (lowest excitation energy) and the number of low energy states for the snapshots of pCT⁻ and Nile Red are shown in Figures 2 and 3, respectively. The trends are quite similar for the two chromophores. The S₀→S₁ transition can be identified as predominantly chromophore→chromophore (closed squares) or CT between water and chromophore (open circles). Because it can be difficult to identify a higher energy purely chromophore→chromophore transition once there is large mixing with water energy levels, energy values of 3.0 and 2.5 eV are chosen for examination of the growth of low energy CT transitions in the bottom panel of the figures.

For CIS and LC- ω PBEh, there is stable behavior with increasing numbers of waters. The S₀→S₁ transition is always chromophore→chromophore, with no water→chromophore transitions appearing at low energies. The pCT⁻ snapshot with 6 Å solvation shell (101 waters) will be used throughout this work as a point of reference, as it seems that any CT transition behavior issues have made themselves present at this degree of

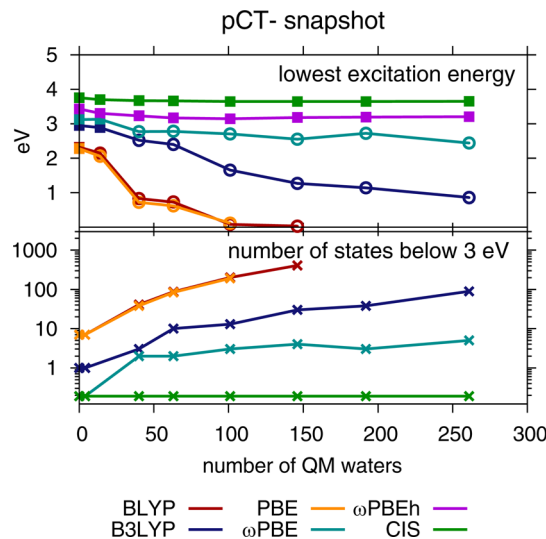


Figure 2. pCT^- snapshot surrounded by increasing numbers of QM waters: the lowest excitation energy $S_0 \rightarrow S_1$ in eV (top) and number of excited states below 3 eV (bottom). The lowest excitation energy is either chromophore→chromophore (closed squares) or water→chromophore (open circles). Both CIS and ωPBEh calculations yield zero states with excitation energies below 3 eV.

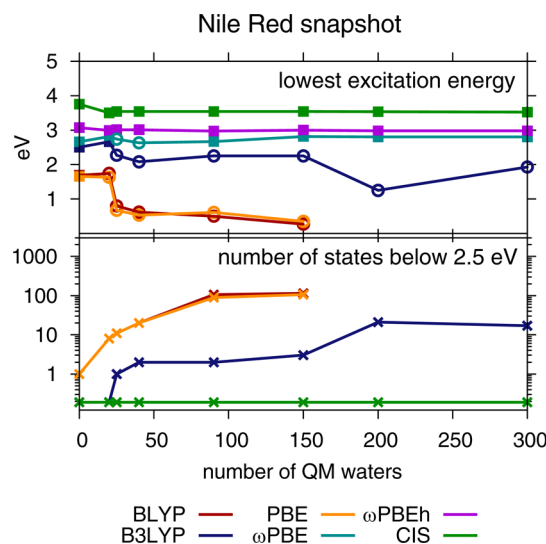


Figure 3. Nile Red snapshot surrounded by increasing numbers of QM waters: the lowest excitation energy $S_0 \rightarrow S_1$ in eV (top) and number of excited states below 2.5 eV (bottom). The lowest excitation is either chromophore→chromophore (closed squares) or water→chromophore (open circles). CIS, ωPBEh , and ωPBE calculations yield zero states with excitation energies below 2.5 eV.

solvation. For this structure, denoted $\text{pCT}\bullet(\text{H}_2\text{O})_{101}$, the onset of the water→chromophore CT transitions are at 3.71 eV with ωPBEh ($S_0 \rightarrow S_3$), which is 0.6 eV above the $S_0 \rightarrow S_1$ transition. For CIS, the lowest energy water→chromophore CT transition is quite high in energy: 8.3 eV ($S_0 \rightarrow S_{22}$), which is 4.7 eV above the chromophore→chromophore bright state $S_0 \rightarrow S_1$ transition, supporting previous studies that show that CIS places CT states too high in energy.²⁹

While CIS and LC- ωPBEh robustly predict that valence excitation of the chromophore is the lowest excited state for increasing numbers of QM water molecules, low-lying CT states plague both LC- ωPBE and hybrid B3LYP (as well as the

semilocal functionals). TDDFT calculations with B3LYP and ωPBE show that with up to ~20 waters the chromophore→chromophore transition remains $S_0 \rightarrow S_1$ for both pCT^- and Nile Red, but with larger solvation shells the lowest state becomes a water→chromophore CT state. The number of low energy CT excitations greatly increases with B3LYP for both chromophores, and also increases for LC- ωPBE with pCT^- . Thus, it appears that long-range correction by itself is not sufficient to keep the solvent→chromophore CT states from falling below the chromophore→chromophore transitions.

The GGA functionals BLYP and PBE give remarkably similar behavior, with both methods showing the characteristic problem of a very large numbers of CT states occurring at spuriously low energies. Both functionals show that the $S_0 \rightarrow S_1$ energy gap closes with solvation of ~100 QM waters. This excited state energy gap closure ultimately leads to problematic ground state SCF convergence, as it is related to highest occupied molecular orbital (HOMO)–lowest unoccupied molecular orbital (LUMO) gap closure. Indeed, the SCF procedure did not converge for snapshots with larger numbers of QM water molecules using these functionals. Such convergence difficulties using pure functionals have been previously observed for large molecules.^{6,8,10} The excited state difference density of the BLYP $S_0 \rightarrow S_1$ transition for the $\text{pCT}\bullet(\text{H}_2\text{O})_{101}$ snapshot is shown in Figure 4. This transition excites an electron from a water molecule at the edge of the cluster to the chromophore, leading to a TD-BLYP/6-31G excitation energy of only 0.08 eV.

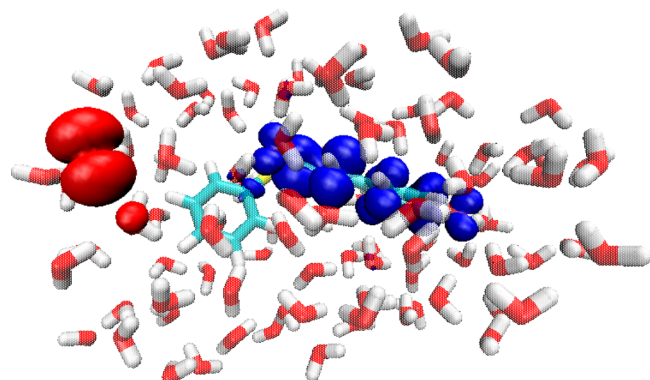


Figure 4. The difference in BLYP/6-31G electron density for the lowest excited state and ground state ($S_0 \rightarrow S_1$ transition) in pCT^- surrounded with 101 QM waters. Electron density is transferred from the edge water (red) to the chromophore (blue). The value of the plotted isosurface is $\pm 8 \times 10^{-6}$.

4.2. The Effect of Aqueous Solvation on the Ground State Orbital Energies.

When either chromophore is solvated by ~100 QM waters, SCF convergence with BLYP and PBE functionals becomes problematic due to a decreasing HOMO–LUMO gap. In order to understand this behavior better, we examined the ground state molecular orbital energies upon solvation. We show the ground state projected density of states (DOS) for the pCT^- snapshot with increasing amounts of QM water computed with BLYP/6-31G in Figure 5. The projected DOS for the water is divided into contributions from the closest 14 water molecules (“inner waters”), and for $\text{pCT}\bullet(\text{H}_2\text{O})_{101}$, the remaining 87 outer water molecules (“outer waters”). Water molecule positions have not been relaxed relative to the snapshot geometry from the MM

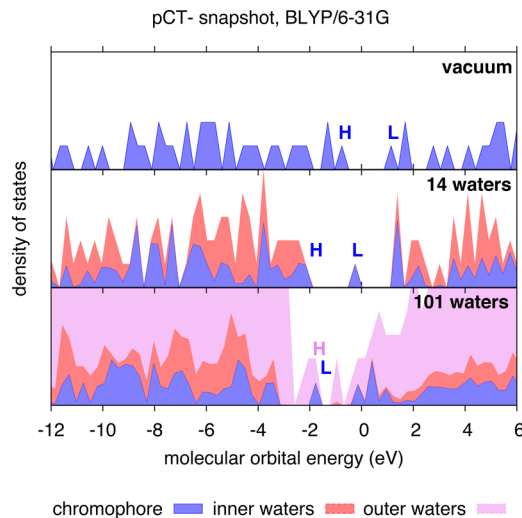


Figure 5. The BLYP/6-31G density of states for pCT^- snapshot in vacuum (top), with 14 QM waters (middle), and with 101 QM waters (bottom). The vacuum geometry is a subset of the 14 water geometry, which is a subset of the 101 water geometry. The highest occupied molecular orbital (HOMO) is indicated with an 'H', and the lowest unoccupied molecular orbital (LUMO) is indicated with an 'L'. The color of the label corresponds to the dominant character of the molecular orbital.

dynamics. The HOMO (denoted by H) and LUMO (denoted by L) are labeled, with their color specifying the dominant orbital contribution. Similar figures for other functionals, for both pCT^- and Nile Red, are available in the Supporting Information, Figures S1–S9.

As seen in Figure 5, with 14 unrelaxed QM water molecules surrounding pCT^- , the occupied water levels are at the same energy as the occupied frontier orbitals of the chromophore. With 101 QM waters (keeping the same 14 inner waters and adding the next closest 87 waters), occupied water levels (primarily localized on water molecules located at the edge of the solvation sphere) are higher in energy than the chromophore occupied levels, and cause a closing of the HOMO–LUMO gap. Hirshfeld charges⁶² computed for the $\text{pCT}\bullet(\text{H}_2\text{O})_{101}$ BLYP electron density show that waters at the edge of the solvation sphere contain a partial negative charge if they act primarily as hydrogen bond donors and a partial positive charge if they are primarily hydrogen bond acceptors (see Figure 6a). These partial charges at the edge of the solvation sphere can be attributed to the snapshot carving process. With an additional layer of water, the hydrogen bond donor waters at the edge would also become hydrogen bond acceptors, balancing their charge distribution. The water molecules responsible for the problematic energy levels that are above the occupied chromophore levels are highlighted in Figure 6b as larger spheres. These water molecules are hydrogen bond donors at the edge of the solvation sphere carrying a partial negative charge ranging from 0.03 e^- to 0.18 e^- .

Because there is no e^-h^+ Coulombic attraction in TDDFT with LDA and GGA functionals, these ground state orbital energies are the dominant factor determining which states are lowest in energy in the TDDFT electronic absorption spectrum. As has been noted by others^{63,64} and is made clear by the ground state DOS in Figure 5, the excited state TDDFT CT problem in aqueous solvation is very much due to a poor

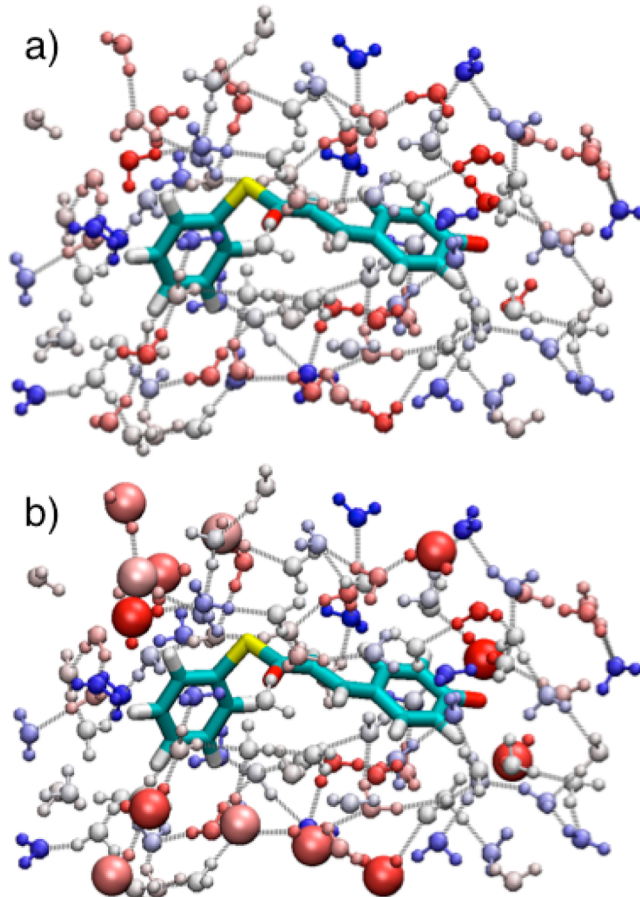


Figure 6. pCT^- with 101 QM waters with hydrogen bonding network highlighted by gray dashes. (a) The Hirshfeld charges for the waters computed with the BLYP electron density of the system are displayed as either red (negative) or blue (positive), with a range of $\pm 0.18 \text{ e}^-$. (b) Oxygen atoms with occupied p-orbitals higher in energy than the highest chromophore orbital are highlighted as larger spheres.

description of the ground state by DFT. It is thus worth investigating the degree to which long-range corrected density functionals might be able to address this problem for solvated molecules.

We present a direct comparison of the ground state DOS for hybrid B3LYP, LC- ω PBE, LC- ω PBEh, and HF/6-31G calculations with the same $\text{pCT}\bullet(\text{H}_2\text{O})_{101}$ unrelaxed snapshot in Figure 7 along with Nile Red and 150 waters in Figure 8. The density functionals and HF give a fairly similar description of the chromophore energy levels, with BLYP giving a much smaller energy gap between chromophore occupied and unoccupied energy levels than HF, as expected based on DFT and HF HOMO–LUMO gap trends. The location of the unoccupied water levels is also fairly consistent across methods, generally being a bit higher in energy than the chromophore LUMO. The key difference between the methods is the location of the occupied water energy levels relative to the chromophore occupied energy levels. While there is no gap closure to the same extent as with BLYP, the other density functionals have occupied exterior water molecular orbital energy levels higher in energy than or equal to the chromophore occupied energy levels. Only HF places the water occupied energy levels lower in energy than the chromophore valence energy levels, suggesting a very different

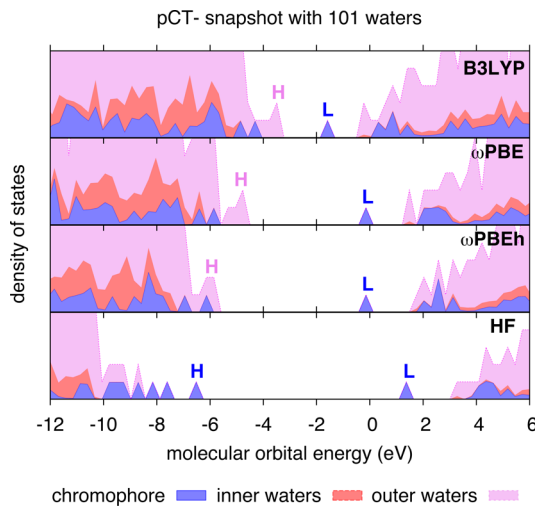


Figure 7. Comparison of B3LYP, ω PBE, ω PBEh, and HF/6-31G density of states with identical pCT⁻ snapshot geometry including 101 surrounding QM waters. HOMO and LUMO indicated as in Figure 5.

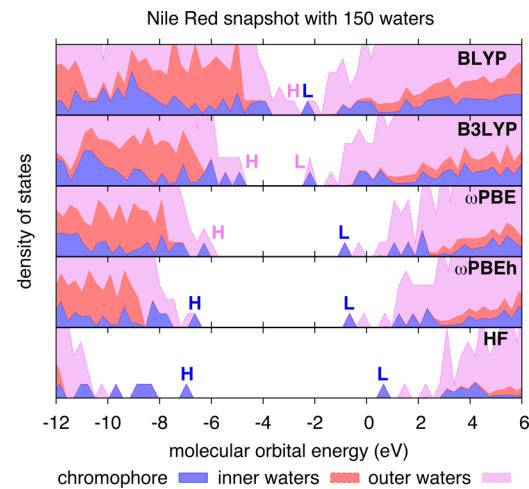


Figure 8. Comparison of BLYP, B3LYP, ω PBE, ω PBEh, and HF/6-31G density of states with identical Nile Red snapshot geometry including 150 surrounding QM waters. HOMO and LUMO indicated as in Figure 5.

treatment of the edge waters by DFT and HF. Hirshfeld charges computed from the HF density predict the charge

distribution of the edge waters to be similar to those from the BLYP density, and thus it is the orbital energies of the hydrogen bond donating waters that are the primary difference.

Stein et al.^{25,26} have suggested that one approach to improving the TDDFT CT excitation energies is tuning the range separation parameter in LC density functionals to obey Koopman's theorem. The value for μ is determined to minimize the difference in the ionization potential (difference in ground state energies of the N and $N-1$ electron systems) and the HOMO energy: $E_{\text{gs}}(N-1, \mu) - E_{\text{gs}}(N, \mu) - \varepsilon^{\mu}_{\text{HOMO}}$. For LC- ω PBE and LC- ω PBEh computations of pCT•(H₂O)₁₀₁, we find that the value of μ that minimizes the difference is $\mu = 0.26$ and $\mu = 0.19$, respectively. These values are quite close to our default value of $\mu = 0.20$, and no substantial difference in the DOS is observed for these values of μ .

The different treatment of these edge waters by DFT and HF likely stems from DFT's delocalization error (electrons tend to be too delocalized) and HF's localization error (electrons tend to be too localized).⁶⁵ The edge waters are unfavorably located compared to the inner waters. They are exposed to vacuum on one side of the droplet and are in a position to hydrogen bond with neighboring waters that were not included in the droplet carving process. Upon examination of highest energy occupied water orbitals, we find that they correspond to the edge waters that are positioned to only act as hydrogen donors (oxygen oriented toward vacuum, hydrogens toward the droplet), and that their acceptor role has been removed by the droplet culling process. These problematic edge donor waters carry too much negative charge compared to the inner waters. DFT predicts that the electrons in the p-orbitals of these donor edge waters are at higher energies than the chromophore HOMO (almost becoming metallic for BLYP), while HF places these p-orbital electrons much lower in energy.

Because the CT problem is generally attributed to the lack of the TDDFT Coulombic $1/r$ dependence between the excited electron and hole, we directly compare the ground state HOMO-LUMO gaps and the TDDFT/CIS excited state $S_0 \rightarrow S_1$ transition energies in Table 1. For the pCT•(H₂O)₁₀₁ snapshot, there is very little change in energy between the HOMO-LUMO gap and the $S_0 \rightarrow S_1$ transition energies for the GGA functionals BLYP and PBE. Thus, the ground state HOMO and LUMO energies are problematic to begin with, and the TDDFT process does not improve the energetics. The remaining density functional methods include some HF

Table 1. Ground State HOMO–LUMO Gaps and TDDFT/CIS First Excited State $S_0 \rightarrow S_1$ Energy (in eV) for pCT⁻ with 101 Quantum Mechanical Waters^a

method	snapshot		6-31++G*		MM water shell		PCM		optimized	
	gap	$S_0 \rightarrow S_1$	gap	$S_0 \rightarrow S_1$	gap	$S_0 \rightarrow S_1$	gap	$S_0 \rightarrow S_1$	gap	$S_0 \rightarrow S_1$
BLYP	0.07	0.08, w→c	1.28	1.28, w→c	0.98	0.98, w→c	1.13	1.14, w→c	1.57	1.57, c→w
PBE	0.02	0.12, w→c	1.19	1.19, w→c	0.87	0.87, w→c	---	---	1.81	1.81, c→w
B3LYP	2.03	1.65, w→c	2.87	2.56, c→c	2.89	2.52, w→c	2.89	2.61, w→c	3.01	2.68, c→c
ω PBE	4.57	2.70, w→c	5.67	2.81, c→c	5.45	2.84, c→c	---	---	5.81	3.11, c→c
ω PBEh	5.64	3.14, c→c	6.17	3.08, c→c	6.10	3.18, c→c	---	---	6.21	3.37, c→c
HF/CIS	8.08	3.64, c→c	7.13	3.58, c→c	8.09	3.65, c→c	8.08	---	8.09	3.74, c→c

^aThe dominant character of the $S_0 \rightarrow S_1$ transition is labeled as chromophore→chromophore (c→c), water→chromophore (w→c), or chromophore→water (c→w). The snapshot geometry includes the 101 water molecules closest to the chromophore carved from an MM dynamics snapshot. The MM water shell geometry is identical to the snapshot geometry but additionally includes 893 MM waters around the QM waters. The optimized geometry keeps the chromophore geometry fixed but optimizes the geometry of the MM waters (using an MM force field). The basis set is 6-31G unless otherwise indicated.

exchange and therefore some Coulombic $1/r$ contribution to the TDDFT energies, and the $S_0 \rightarrow S_1$ energy gap is smaller than the ground state band gap.

For snapshot computations with BLYP, PBE, LC- ω PBE, and B3LYP, the lowest excited state, as predicted from either HOMO and LUMO character or direct analysis of the TDDFT-predicted $S_0 \rightarrow S_1$ transition, excites an electron from a water molecule to the chromophore. Thus, the comparison is a measure of how much TDDFT corrects the water→chromophore energy gap. For BLYP and PBE, the change is little, if any. Table 1 shows that for B3LYP and LC- ω PBE, the difference in energy between the HOMO–LUMO gap and the $S_0 \rightarrow S_1$ energy is 0.4 and 1.9 eV, respectively. In contrast, the stabilization for the higher energy chromophore→chromophore transition (not shown) remains 0.4 eV for B3LYP, but increases to ~2.5 eV for LC- ω PBE, indicating that the LC functional is correctly stabilizing the proximal excited chromophore electron–hole pair more than the distant water–chromophore electron–hole CT state. However, this larger stabilization is not enough to make the chromophore→chromophore transition lower than the water→chromophore transitions.

For LC- ω PBEh a HOMO to LUMO transition would excite an electron from an edge water molecule to the chromophore, but the TD-LC- ω PBEh $S_0 \rightarrow S_1$ transition is dominated by chromophore→chromophore contributions. The stabilization of the chromophore→chromophore and water→chromophore transitions is similar to that of LC- ω PBE, and since the occupied outer water energy levels are at lower energies, this stabilization is enough to keep the chromophore→chromophore transitions as the lowest excited states. For HF/CIS the stabilization is very large: the energy for the chromophore→chromophore $S_0 \rightarrow S_1$ transition is 4.4 eV smaller than the HOMO–LUMO gap. The CIS transitions between water and the chromophore are stabilized by approximately half this amount.

In summary, the energetics of the edge donor water occupied molecular orbital energy levels are very different in HF and DFT. For DFT, these orbitals are at higher energies than the chromophore occupied orbitals, and water→chromophore CT transitions are the lowest energy transitions computed by TDDFT. While these water occupied orbitals remain at higher energies than the chromophore orbitals for the LC functionals, a large amount of HF exchange, as in the LC- ω PBEh functional, adds enough e^-h^+ Coulomb stabilization to keep the chromophore→chromophore valence transitions as the lowest energy TDDFT transitions.

4.3. Basis Set Effects. By increasing the quality of the basis set from 6-31G to 6-31++G*, we find that the ground state HOMO–LUMO gap problem is improved. Table 1 shows that for the pCT•(H₂O)₁₀₁ snapshot, the gap for BLYP, PBE, and LC- ω PBE increases by more than 1 eV; the increase for the other functionals is more modest. The band gap increase translates into a substantial increase in the $S_0 \rightarrow S_1$ transition energy for BLYP, PBE, and B3LYP, while LC- ω PBE undergoes only a slight increase, and the $S_0 \rightarrow S_1$ transition energy decreases slightly (by 0.06 eV) for LC- ω PBEh and CIS.

The plot of the density of states with the 6-31++G* basis set for pCT⁻ in Figure 9 and for Nile Red in Figure S10 shows that the chromophore orbital energies are not substantially different than with the 6-31G basis set, but both the occupied and unoccupied edge waters undergo large shifts to lower energies. This shift to lower energies places the occupied edge water

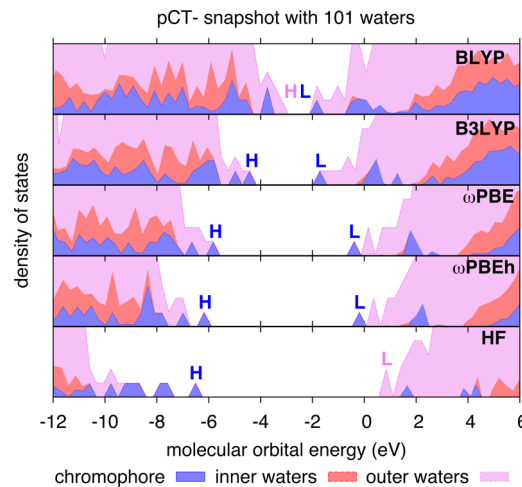


Figure 9. Comparison of BLYP, B3LYP, ω PBE, ω PBEh, and HF/6-31++G* density of states with identical pCT⁻ snapshot geometry including 101 surrounding QM waters. HOMO and LUMO indicated as in Figure 5.

levels below the chromophore HOMO level for all functionals with some HF exchange. One rationale for the added stability of these edge water levels is that the extra basis functions give the oxygen p-orbitals enough flexibility to polarize toward the droplet rather than the vacuum, decreasing their overall energy relative to the chromophore occupied levels. With a larger basis set there are more unoccupied energy levels, and we see that these new unoccupied water energy levels approach the chromophore LUMO level, so much so that with HF the edge water levels are lower in energy than the chromophore LUMO.

These changes in the orbital energy levels lead to slightly more stable TDDFT behavior (see Figure S11 in the Supporting Information). The number of low-energy states does not rise quite as sharply for BLYP and PBE. The lowest energy TD-B3LYP transitions remain chromophore→chromophore through 100 QM waters, but become CT with larger numbers of water molecules. The TD-LC- ω PBE lowest energy transition remains chromophore→chromophore with solvation by 192 QM waters.

4.4. The Effect of Water Relaxation. All preceding results were from an MM dynamics snapshot in which the closest water molecules were cut out of a much larger solvation box (since periodic boundary conditions were used in the MM dynamics). The waters were not relaxed and were in a position to interact with nearby waters that were removed in the culling procedure. The lowest energy (and thus most problematic) water→chromophore excited state transitions involve these waters at the edge of the solvation shell that act only as hydrogen donors, not acceptors. As the solvation shell gets larger, there are more of these waters at the edge, increasing the number of edge water states. We will show that the degree of the CT problem can be greatly affected not just by the number of edge waters, but also by their particular configurations.

While holding the chromophore fixed in the snapshot geometry, the geometry of the water shell was optimized within AMBER, using the same TIP3P parameters for the water as in the original dynamics. Since each snapshot was optimized individually, the water shell geometries were no longer strict subsets of each other. As seen in Table 1, the optimization led to a widening of the HOMO–LUMO gap and an increase of

the $S_0 \rightarrow S_1$ transition energy for all density functional methods. The HF HOMO–LUMO gap and the CIS/LC- ω PBEh $S_0 \rightarrow S_1$ excitation energies were not greatly affected, as these involved chromophore→chromophore transitions even before relaxation. Not only is the HOMO–LUMO gap widened for DFT methods, but the occupied water orbitals now occur at lower energies than the chromophore occupied orbitals for all methods, as shown for pCT⁻ in Figure 10 (Figure S12 for Nile Red). Relaxation of the waters via equilibration procedures showed similar behavior (not shown).

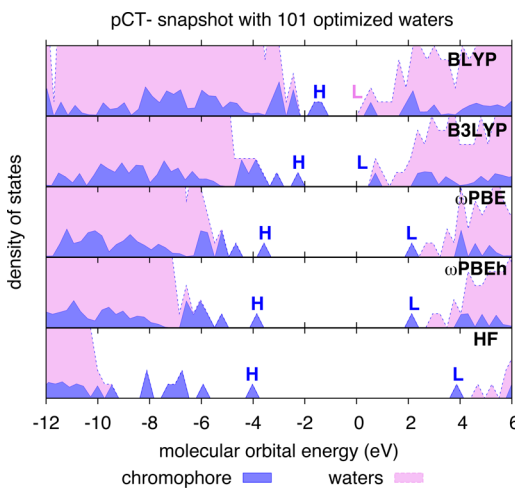


Figure 10. Comparison of BLYP, B3LYP, ω PBE, ω PBEh, and HF/6-31G density of states with identical pCT⁻ snapshot geometry where the positions of the 101 surrounding QM waters have been optimized. HOMO and LUMO indicated as in Figure 5. See Figure S12 for comparable figure for Nile Red.

The improved HOMO–LUMO gap and excited state energetics upon optimization of the water molecules (see Figure S13 for TDDFT plot) indicates that their orientation as carved from bulk water can significantly exacerbate the CT problem in TDDFT. Without their hydrogen bonding water partners, the water oxygen p-orbital energy levels are unstable and close to the chromophore HOMO. After optimization, the waters have increased hydrogen bonding interactions with each other, and the oxygen p-orbital levels are stabilized. This pushes the water→chromophore CT states to higher energies, where they overlap less with the chromophore→chromophore valence transitions. However, from the density of states in Figure 10, it is also clear that the unoccupied water energy levels are lowered upon optimization. This brings the water energy levels very close to the chromophore LUMO level, especially for the GGA functionals and B3LYP. These lower energy unoccupied water levels change the nature of the problematic CT states from being water→chromophore to chromophore→water.

4.5. The Effect of External Environment. There are strong edge effects related to the solvation TDDFT CT problem. A ‘quick fix’ has been noted by Herbert and co-workers: they found that the CT problem was ameliorated by surrounding the QM water shell with MM waters, which are represented by point charges embedded in the QM Hamiltonian.²⁰ This external charged environment pushes the low-energy spurious CT states to higher energies. Here we compare the efficacy of this approach in reducing the CT excited states with the effects of surrounding the QM droplet subsystem with a polarizable continuum, and with using

periodic boundary conditions (PBCs). The results reconcile some of the conflict observed between the atom-centered basis community, who find the CT problem rampant, and the plane-wave community, who have found the CT problem to be less grievous.

MM Point Charges. For each solute, all water molecules in the primary cell from the MM dynamics snapshot were included, with the closest water molecules treated as QM, and the surrounding waters as MM point charges. As shown in Figures 11 and S14, external point charges stabilize the edge

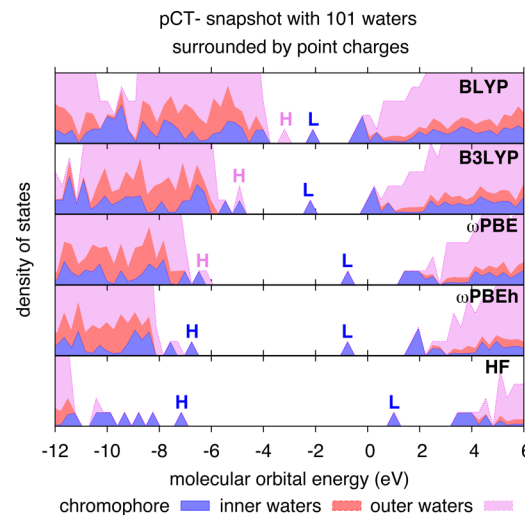


Figure 11. Comparison of BLYP, B3LYP, ω PBE, ω PBEh, and HF/6-31G density of states with identical pCT⁻ snapshot geometry where the 101 QM water molecules are surrounded by MM water point charges. HOMO and LUMO indicated as in Figure 5.

donor waters enough to widen the HOMO–LUMO gap of pCT⁻(H₂O)₁₀₁ by almost 1 eV for the GGA and hybrid density functionals. For LC- ω PBEh the stabilization is ~0.5 eV, while there is no stabilization with HF because the water orbitals are not near the band gap. For all tested functionals, adding the point charges of the MM waters around the solvation cluster decreases the energy of the water occupied orbitals near the chromophore’s HOMO level. This energetic lowering increases the energy of the CT states and increases the DFT band gap.

The DFT band gap increase is not quite as much as for optimization of the waters or for increasing the basis set size to 6-31++G*; see Table 1. TDDFT excitation energies are still problematic for GGA functionals and for B3LYP (Figure S15). However, it does appear that the point charges stabilize the energy levels sufficiently that LC- ω PBE shows no signs of low-energy water→chromophore CT states below the bright chromophore → chromophore transition.

Polarizable Continuum Model. Figure 12 shows the computed BLYP, B3LYP, and HF DOS for the pCT⁻(H₂O)₁₀₁ snapshot using PCM as an alternative description of the charge density surrounding the cluster. The results are comparable to those obtained with explicit point charges, with a widening of the band gap that is slightly larger than that effected by MM point charges, but still shy of the expanded basis and optimized results. The observed reduction in the number of spurious low lying states was also comparable to the MM case, with the lowest lying chromophore→chromophore valence excited state for BLYP appearing as S_{51} and S_{49} for PCM and MM, respectively, and for B3LYP as S_3 in both cases. We did not

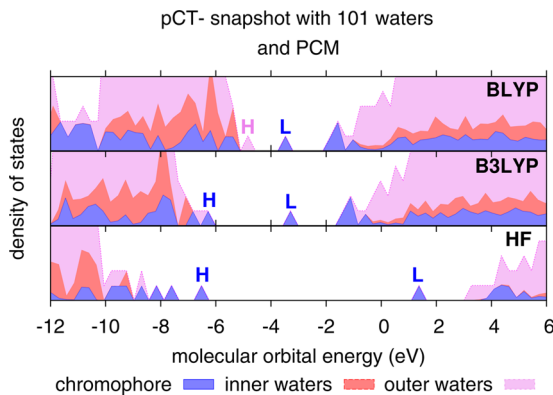


Figure 12. Comparison of BLYP, B3LYP, and HF/6-31G density of states with identical pCT⁻ snapshot geometry in which 101 QM waters are surrounded by a polarizable dielectric continuum.

investigate PCM calculations for the LC- ω PBE and LC- ω PBEEh functionals, as these were not available in GAMESS.

Periodic Boundary Conditions. For the PBC calculations on the system comparable to pCT⁻(H₂O)₁₀₁ snapshot (large box with vacuum around the 101 waters, see Computational Details for more information), the BLYP/plane wave band gap and lowest excited state results are comparable to the BLYP/6-31++G* results (see Table 2). The PBC vacuum calculations

Table 2. Plane Wave Basis Set BLYP Ground State Band Gaps and TD-BLYP First Excited State S₀→S₁ Energies (in eV) for pCT⁻ with Quantum Mechanical Waters^a

environment	basis set	gap	S ₀ →S ₁	c → c?
vacuum (101 waters)	6-31++G*	1.28	1.28	no
PBCs with vacuum (101 waters)	pw (90 Ry)	1.57	1.57	no
PBCs with liquid (385 waters)	pw (90 Ry)	1.40	2.04	yes
PBCs with bubble (380 waters, a) ^b	pw (90 Ry)	1.45	1.69	no
PBCs with bubble (380 waters, b) ^c	pw (90 Ry)	1.04	1.23	no
PBCs with bubble (375 waters, a) ^b	pw (90 Ry)	0.32	0.50	no
PBCs with bubble (375 waters, b) ^c	pw (90 Ry)	0.92	1.09	no
PBCs with bubble (375 waters, c) ^c	pw (90 Ry)	1.32	1.56	no
PBCs with bubble (375 waters, d) ^c	pw (90 Ry)	1.45	1.83	no
PBCs with bubble (375 waters, e) ^c	pw (90 Ry)	1.20	1.39	no

^aWhether or not the S₀→S₁ transition is dominated by chromophore → chromophore character (c → c) is indicated. The chromophore is fixed in the geometry of the previous computations. A plane wave (pw) basis set with a cutoff of 90 Ry is used for the PBC computations. See Figure S16 for bubble geometries a-e in the 375 water system. ^bNonspherical bubble at the edge of the box (distance of 7.4 Å from the chromophore). ^cConstruction of bubbles was a symmetric 3.2 to 3.7 Å hole around different water molecules close to the edge of box. Distance from the bubble to the chromophore is between 3.8 Å to 4.7 Å. This was performed for two different water sites with the 380 water molecule calculation and at four different water sites with 375 surrounding water molecules.

gave a band gap and lowest excitation energy of 1.57 eV; as with the water clusters examined previously, this lowest excited state transfers an electron from an edge water to the chromophore. Thus, as can be gleaned from the Gaussian basis set calculations reported above, finite basis effects are not the sole contributor to the CT problem.

The second PBC system is a simulation in ‘liquid water’ (no vacuum or edge effects, see Figure 13, left). It is important to

stress that in our simulations the gap of liquid water is unphysically small because of the use of classical structures in combination with GGA/(TD-)DFT energy calculations. Indeed, by relaxing the structure of pure water with Car-Parrinello dynamics the HOMO–LUMO gap of liquid water increases from 2.0 eV to around 5.0 eV.⁶⁶ With pCT⁻ solvated in liquid water, the gap and CT situation is quite different from a cluster calculation. The HOMO–LUMO gap is smaller (1.40 eV), but the TD-BLYP lowest excitation energy is 2.04 eV (0.6 eV larger than the band gap). This simulation allows for a classical equilibration of the water molecules and avoids any “edge waters” by using PBCs. This further strengthens the conclusions above that the “edge water” molecules are responsible for exacerbating the CT problem in cluster calculations.

In order to further show that the edge water molecules are at the root of the CT problem, we have constructed a third series of systems to be studied with PBCs and a plane wave basis set. In these systems, we introduce a ‘bubble’ in the solvent by removing a subset of water molecules (two, five, or ten). The results remain comparable to the liquid water case only for the smallest hole (two waters removed). When five or ten waters are removed, the lowest TD-BLYP excitation energy drops below 2.04 eV (see Table 2) because of the appearance of defect states in the gap (see density of states Figure S17). The transition gains CT character as the waters at the edge of the ‘bubble’ lose their hydrogen bonding partners and then become involved in the lowest energy excitation (see Figure 13, right).

5. CONCLUSIONS

We have shown that, for approximate density functionals, the cause of low-energy CT excited states when performing TDDFT calculations of a solute with QM water molecules can be largely traced back to a decreasing HOMO–LUMO gap in ground state DFT for systems with “edge waters” that are unsaturated and robbed of their hydrogen bonding partner. Edge waters that are hydrogen bond donors to the remainder of the cluster (oxygen atoms pointing toward vacuum) can be singled out as the primary contributors to the decreasing HOMO–LUMO gap. The CT problem associated with these edge waters is exacerbated when their geometry is nonoptimal, the basis set is not large enough, electrostatic stabilization is not included, and/or the functional does not include full strength long-range HF exchange.

The CT problem is thus not only due to neglect of Coulombic e⁻h⁺ attraction, but also due to incorrect placement of the orbital energies for “edge waters” compared to chromophore orbital energies. There may even be a closing of the HOMO–LUMO gap in larger solvation spheres since GGA functionals predict very high occupied orbital energies for these unsaturated water molecules. For functionals with some HF exchange such as hybrid and LC functionals, these hydrogen bond donor water occupied energy levels are significantly stabilized. This, along with some percentage of the proper Coulombic e⁻h⁺ interaction in the excited states, raises the energy of water→chromophore and chromophore→water CT excited states in hybrid and LC TDDFT calculations. Even so, with sufficiently large solvation spheres (~100 QM waters), these CT states often fall below the lowest chromophore→chromophore valence transitions in hybrid B3LYP and LC- ω PBE TDDFT computations. The LC- ω PBEEh functional has 20% HF exchange at short-range, which further decreases the energy of the occupied water

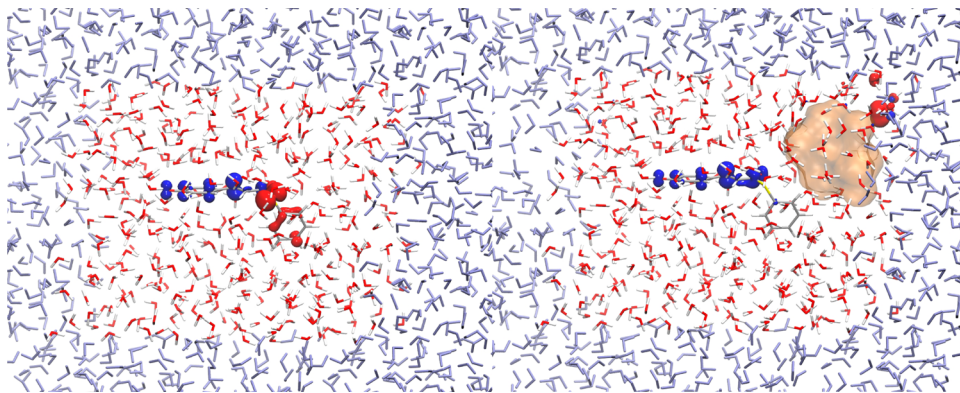


Figure 13. pCT^- surrounded by 385 waters for liquid water system (left) and 375 waters for a bubble system (right) within a PBC setup (for reasons of clarity, the periodicity is only reproduced in the xy plane, with replicated water molecules represented in light blue). Difference density for the $S_0 \rightarrow S_1$ transition is represented by isosurfaces (negative contribution = red, positive contribution = blue). The empty ‘bubble’ region for the 375 waters structure is highlighted with an orange transparent surface.

orbital energy levels relative to the chromophore orbital energy levels. The LC- ω PBEh TDDFT lowest energy excited states remained chromophore \rightarrow chromophore, even with a ~ 300 QM water solvation sphere, and we cautiously recommend this functional for excited state studies that involve solvation with explicit QM waters.

Our work also indicates that the popular solvation technique of culling a QM solvation sphere from a larger solvation model is especially problematic for DFT and TDDFT. The edge waters are in a position to hydrogen bond with neighboring waters outside the cutoff distance, and a DFT calculation places the occupied hydrogen bond donor edge water orbitals very high in energy, leading to low-energy water \rightarrow chromophore CT transitions. Optimization of water molecule positions stabilizes these water orbital energy levels, increasing the energy of the water \rightarrow chromophore CT transitions.

In addition to geometry relaxation, we have explored other methods of improving the energetics of these edge waters. A larger basis set gives more flexibility to the occupied oxygen p-orbitals, lowering their energy relative to the chromophore HOMO levels. However, the additional unoccupied water energy levels then approach the chromophore LUMO levels, resulting in lower energy chromophore \rightarrow water CT transitions that encroach on the valence chromophore \rightarrow chromophore transitions for functionals with minimal or no HF exchange. Another route to improved behavior is the technique proposed by the Herbert group of surrounding the QM water solvation sphere with MM water point charges.²⁰ The hybrid B3LYP functional still shows some low energy CT states with this technique, but the LC- ω PBE functional performs well with 250+ QM waters. Tests on the BLYP and B3LYP functionals with a polarizable continuum showed similar stabilization as with MM water point charges. BLYP calculations with PBCs that remove all edge effects do not have low energy CT states, but similar problems arise if edges are introduced via a ‘bubble’ in the solvent box, or if PBCs are used with a water/vacuum interface.

This work explains the contrast between perceptions of the CT problem in the atom-centered and plane wave basis set communities. Since unsaturated “edge waters” are rarely encountered in periodic calculations intended to mimic solvated systems, the CT problem is less egregious in the context of plane wave calculations. Our work also points out the weaknesses (in the context of DFT and TDDFT) of the

common approach that evaluates electronic properties using snapshot geometries cut out from larger dynamics simulations. In view of the HOMO–LUMO gap problems that we have shown here, one can only recommend this approach if it is followed by some form of geometric relaxation and/or description of the surrounding environment. Even then, hybrid functionals that include full strength long-range HF exchange should be used (such as LC- ω PBEh).

■ ASSOCIATED CONTENT

Supporting Information

The Cartesian coordinates of all structures in this work, as well as additional figures described in the text. This material is available free of charge via the Internet at <http://pubs.acs.org>.

■ AUTHOR INFORMATION

Corresponding Author

*E-mail: cisborn@ucmerced.edu. Phone: (209) 228-4693.

Notes

The authors declare no competing financial interest.

■ ACKNOWLEDGMENTS

This work was supported by NSF (CHE-10-47577) and the Department of Defense (Office of the Director of Defense Research and Engineering) through a National Security Science and Engineering Faculty Fellowship. This research used computational resources provided through DOE Contract No. DE-AC02-7600515.

■ REFERENCES

- (1) Ufimtsev, I. S.; Martinez, T. J. Quantum Chemistry on Graphical Processing Units. 1. Strategies for Two-Electron Integral Evaluation. *J. Chem. Theory Comput.* **2008**, *4*, 222–231.
- (2) Ufimtsev, I. S.; Martinez, T. J. Quantum Chemistry on Graphical Processing Units. 2. Direct Self-Consistent-Field Implementation. *J. Chem. Theory Comput.* **2009**, *5*, 1004–1015.
- (3) Ufimtsev, I. S.; Martinez, T. J. Quantum Chemistry on Graphical Processing Units. 3. Analytical Energy Gradients, Geometry Optimization, and First Principles Molecular Dynamics. *J. Chem. Theory Comput.* **2009**, *5*, 2619–2628.
- (4) Luehr, N.; Ufimtsev, I. S.; Martinez, T. J. Dynamic Precision for Electron Repulsion Integral Evaluation on Graphical Processing Units (GPUs). *J. Chem. Theory Comput.* **2011**, *7*, 949–954.
- (5) Hine, N. D. M.; Haynes, P. D.; Mostofi, A. A.; Skylaris, C. K.; Payne, M. C. Linear-scaling density-functional theory with tens of

- thousands of atoms: Expanding the scope and scale of calculations with ONETEP. *Comput. Phys. Commun.* **2009**, *180*, 1041–1053.
- (6) Rudberg, E. Difficulties in applying pure Kohn–Sham density functional theory electronic structure methods to protein molecules. *J. Phys.: Condens. Matter* **2012**, *24*, 072202.
- (7) Ufimtsev, I. S.; Luehr, N.; Martinez, T. J. Charge Transfer and Polarization in Solvated Proteins from Ab Initio Molecular Dynamics. *J. Phys. Chem. Lett.* **2011**, *2*, 1789–1793.
- (8) Kulik, H. J.; Luehr, N.; Ufimtsev, I. S.; Martinez, T. J. Ab Initio Quantum Chemistry for Protein Structures. *J. Phys. Chem. B* **2012**, *116*, 12501–12509.
- (9) Isborn, C. M.; Götz, A. W.; Clark, M. A.; Walker, R. C.; Martínez, T. J. Electronic Absorption Spectra from MM and ab Initio QM/MM Molecular Dynamics: Environmental Effects on the Absorption Spectrum of Photoactive Yellow Protein. *J. Chem. Theory Comput.* **2012**, *8*, 5092–5106.
- (10) Isborn, C. M.; Luehr, N.; Ufimtsev, I. S.; Martinez, T. J. Excited-State Electronic Structure with Configuration Interaction Singles and Tamm–Dancoff Time-Dependent Density Functional Theory on Graphical Processing Units. *J. Chem. Theory Comput.* **2011**, *7*, 1814–1823.
- (11) Cramer, C. J.; Truhlar, D. G. Implicit Solvation Models: Equilibria, Structure, Spectra, and Dynamics. *Chem. Rev.* **1999**, *99*, 2161–2200.
- (12) Tomasi, J.; Mennucci, B.; Cammi, R. Quantum Mechanical Continuum Solvation Models. *Chem. Rev.* **2005**, *105*, 2999–3094.
- (13) Runge, E.; Gross, E. K. U. Density-Functional Theory for Time-Dependent Systems. *Phys. Rev. Lett.* **1984**, *52*, 997.
- (14) Dreuw, A.; Weisman, J. L.; Head-Gordon, M. Long-range charge-transfer excited states in time-dependent density functional theory require non-local exchange. *J. Chem. Phys.* **2003**, *119*, 2943–2946.
- (15) Dreuw, A.; Head-Gordon, M. Single-Reference ab Initio Methods for the Calculation of Excited States of Large Molecules. *Chem. Rev.* **2005**, *105*, 4009–4037.
- (16) Tozer, D. J. Relationship between long-range charge-transfer excitation energy error and integer discontinuity in Kohn–Sham theory. *J. Chem. Phys.* **2003**, *119*, 12697–12699.
- (17) Bernasconi, L.; Sprik, M.; Hutter, J. Time dependent density functional theory study of charge-transfer and intramolecular electronic excitations in acetone–water systems. *J. Chem. Phys.* **2003**, *119*, 12417–12431.
- (18) Neugebauer, J.; Louwerse, M. J.; Baerends, E. J.; Wesolowski, T. A. The merits of the frozen-density embedding scheme to model solvatochromic shifts. *J. Chem. Phys.* **2005**, *122*, 094115–094113.
- (19) Neugebauer, J.; Gritsenko, O.; Baerends, E. J. Assessment of a simple correction for the long-range charge-transfer problem in time-dependent density-functional theory. *J. Chem. Phys.* **2006**, *124*, 214102–214111.
- (20) Lange, A.; Herbert, J. M. Simple Methods To Reduce Charge-Transfer Contamination in Time-Dependent Density-Functional Calculations of Clusters and Liquids. *J. Chem. Theory Comput.* **2007**, *3*, 1680–1690.
- (21) Casida, M. E. *Recent Advances in Density Functional Methods*; World Scientific: Singapore, 1995.
- (22) Tawada, Y.; Tsuneda, T.; Yanagisawa, S.; Yanai, T.; Hirao, K. A long-range-corrected time-dependent density functional theory. *J. Chem. Phys.* **2004**, *120*, 8425–8433.
- (23) Rohrdanz, M. A.; Herbert, J. M. Simultaneous benchmarking of ground- and excited-state properties with long-range-corrected density functional theory. *J. Chem. Phys.* **2008**, *129*, 034107–034109.
- (24) Rohrdanz, M. A.; Martins, K. M.; Herbert, J. M. A long-range-corrected density functional that performs well for both ground-state properties and time-dependent density functional theory excitation energies, including charge-transfer excited states. *J. Chem. Phys.* **2009**, *130*, 054112–054118.
- (25) Stein, T.; Kronik, L.; Baer, R. Prediction of charge-transfer excitations in coumarin-based dyes using a range-separated functional tuned from first principles. *J. Chem. Phys.* **2009**, *131*, 244119–244115.
- (26) Stein, T.; Kronik, L.; Baer, R. Reliable Prediction of Charge Transfer Excitations in Molecular Complexes Using Time-Dependent Density Functional Theory. *J. Am. Chem. Soc.* **2009**, *131*, 2818–2820.
- (27) Korzdorfer, T.; Sears, J. S.; Sutton, C.; Bredas, J.-L. Long-range corrected hybrid functionals for pi-conjugated systems: Dependence of the range-separation parameter on conjugation length. *J. Chem. Phys.* **2011**, *135*, 204107.
- (28) Karolewski, A.; Stein, T.; Baer, R.; Kummel, S. Communication: Tailoring the optical gap in light-harvesting molecules. *J. Chem. Phys.* **2011**, *134*, 151101–151104.
- (29) Subotnik, J. E. Communication: Configuration interaction singles has a large systematic bias against charge-transfer states. *J. Chem. Phys.* **2011**, *135*, 071104–071104.
- (30) Hoff, W. D.; Dux, P.; Hard, K.; Devreese, B.; Nugteren-Roodzant, I. M.; Crielaard, W.; Boelens, R.; Kaptein, R.; Beeumens, J. V.; Hellingwerf, K. J. Thiol ester-linked p-coumaric acid as a new photoactive prosthetic group in a protein with rhodopsin-like photochemistry. *Biochemistry* **1994**, *33*, 13959–13962.
- (31) Baca, M.; Borgstahl, G. E. O.; Boissinot, M.; Burke, P. M.; Williams, D. R.; Slater, K. A.; Getzoff, E. D. Complete Chemical Structure of Photoactive Yellow Protein: Novel Thioester-Linked 4-Hydroxycinnamyl Chromophore and Photocycle Chemistry. *Biochemistry* **1994**, *33*, 14369–14377.
- (32) van der Horst, M. A.; Hellingwerf, K. J. Photoreceptor proteins, “star actors of modern times”: a review of the functional dynamics in the structure of representative members of six different photoreceptor families. *Acc. Chem. Res.* **2004**, *37*, 13–20.
- (33) Deye, J. F.; Berger, T. A.; Anderson, A. G. Nile Red as a solvatochromic dye for measuring solvent strength in normal liquids and mixtures of normal liquids with supercritical and near critical fluids. *Anal. Chem.* **1990**, *62*, 615–622.
- (34) Dutta, A. K.; Kamada, K.; Ohta, K. Langmuir–Blodgett films of nile red: a steady-state and time-resolved fluorescence study. *Chem. Phys. Lett.* **1996**, *258*, 369–375.
- (35) Dutta, A. K.; Kamada, K.; Ohta, K. Spectroscopic studies of nile red in organic solvents and polymers. *J. Photochem. Photobiol. A* **1996**, *93*, 57–64.
- (36) Gromov, E. V.; Burghardt, I.; Hynes, J. T.; Köppel, H.; Cederbaum, L. S. Electronic structure of the photoactive yellow protein chromophore: Ab initio study of the low-lying excited singlet states. *J. Photochem. Photobiol. A* **2007**, *190*, 241–257.
- (37) Gromov, E. V.; Burghardt, I.; Köppel, H.; Cederbaum, L. S. Impact of Sulfur vs Oxygen on the Low-Lying Excited States of trans-p-Coumaric Acid and trans-p-Coumaric Thio Acid. *J. Phys. Chem. A* **2005**, *109*, 4623–4631.
- (38) Gromov, E. V.; Burghardt, I.; Köppel, H.; Cederbaum, L. S. Electronic Structure of the PYP Chromophore in Its Native Protein Environment. *J. Am. Chem. Soc.* **2007**, *129*, 6798–6806.
- (39) Bravaya, K. B.; Grigorenko, B. L.; Nemukhin, A. V.; Krylov, A. I. Quantum Chemistry Behind Bioimaging: Insights from Ab Initio Studies of Fluorescent Proteins and Their Chromophores. *Acc. Chem. Res.* **2011**, *45*, 265–275.
- (40) Rocha-Rinza, T.; Christiansen, O.; Rajput, J.; Gopalan, A.; Rahbek, D. B.; Andersen, L. H.; Bochenkova, A. V.; Granovsky, A. A.; Bravaya, K. B.; Nemukhin, A. V.; Christiansen, K. L.; Nielsen, M. B. n. Gas Phase Absorption Studies of Photoactive Yellow Protein Chromophore Derivatives. *J. Phys. Chem. A* **2009**, *113*, 9442–9449.
- (41) Zuev, D.; Bravaya, K. B.; Crawford, T. D.; Lindh, R.; Krylov, A. I. Electronic structure of the two isomers of the anionic form of p-coumaric acid chromophore. *J. Chem. Phys.* **2011**, *134*, 034310.
- (42) Nielsen, I. B.; Boyé-Péronne, S.; El Ghazaly, M. O. A.; Kristensen, M. B.; Bröndsted Nielsen, S.; Andersen, L. H. Absorption Spectra of Photoactive Yellow Protein Chromophores in Vacuum. *Biophys. J.* **2005**, *89*, 2597–2604.
- (43) Wang, Y.; Li, H. Excited state geometry of photoactive yellow protein chromophore: A combined conductorlike polarizable continuum model and time-dependent density functional study. *J. Chem. Phys.* **2010**, *133*, 034108.

- (44) Owen Tuck, P.; Christopher Mawhinney, R.; Rappon, M. An ab initio and TD-DFT study of solvent effect contributions to the electronic spectrum of Nile Red. *Phys. Chem. Chem. Phys.* **2009**, *11*, 4471–4480.
- (45) Bergsma, J. P.; Berens, P. H.; Wilson, K. R.; Fredkin, D. R.; Heller, E. J. Electronic spectra from molecular dynamics: a simple approach. *J. Phys. Chem.* **1984**, *88*, 612–619.
- (46) Wohlgemuth, M.; BonaCic-Koutecky, V.; Mitric, R. Time-dependent density functional theory excited state nonadiabatic dynamics combined with quantum mechanical/molecular mechanical approach: Photodynamics of indole in water. *J. Chem. Phys.* **2011**, *135*, 054105–054110.
- (47) AMBER Home Page; <http://ambermd.org/> (accessed August 13, 2013).
- (48) Jorgensen, W. L.; Chandrasekhar, J.; Madura, J. D.; Impey, R. W.; Klein, M. L. Comparison of simple potential functions for simulating liquid water. *J. Chem. Phys.* **1983**, *79*, 926–935.
- (49) Becke, A. D. Density-functional exchange-energy approximation with correct asymptotic behavior. *Phys. Rev. A* **1988**, *38*, 3098.
- (50) Lee, C.; Yang, W.; Parr, R. G. Development of the Colle-Salvetti correlation-energy formula into a functional of the electron density. *Phys. Rev. B* **1988**, *37*, 785.
- (51) Perdew, J. P.; Burke, K.; Wang, Y. Generalized gradient approximation for the exchange-correlation hole of a many-electron system. *Phys. Rev. B* **1996**, *54*, 16533–16539.
- (52) Becke, A. D. Density-Functional Thermochemistry 0.3. The Role of Exact Exchange. *J. Chem. Phys.* **1993**, *98*, 5648–5652.
- (53) Vydrov, O. A.; Heyd, J.; Krukau, A. V.; Scuseria, G. E. Importance of short-range. *Chem. Phys.* **2006**, *125*, 074106.
- (54) Vydrov, O. A.; Scuseria, G. E. Assessment of a long-range corrected hybrid functional. *J. Chem. Phys.* **2006**, *125*, 234109.
- (55) TeraChem Home Page; <http://www.petachem.com> (accessed August 13, 2013).
- (56) Hirata, S.; Head-Gordon, M. Time-dependent density functional theory within the Tamm-Dancoff approximation. *Chem. Phys. Lett.* **1999**, *314*, 291–299.
- (57) Barone, V.; Cossi, M. Quantum Calculation of Molecular Energies and Energy Gradients in Solution by a Conductor Solvent Model. *J. Phys. Chem. A* **1998**, *102*, 1995–2001.
- (58) Cossi, M.; Barone, V. Time-dependent density functional theory for molecules in liquid solutions. *J. Chem. Phys.* **2001**, *115*, 4708–4717.
- (59) Schmidt, M. W.; Baldridge, K. K.; Boatz, J. A.; Elbert, S. T.; Gordon, M. S.; Jensen, J. H.; Koseki, S.; Matsunaga, N.; Nguyen, K. A.; Su, S.; Windus, T. L.; Dupuis, M.; Montgomery, J. A. General atomic and molecular electronic structure system. *J. Comput. Chem.* **1993**, *14*, 1347–1363.
- (60) CPMD Home Page; <http://www.cpmd.org> (accessed August 13, 2013).
- (61) Troullier, N.; Martins, J. L. Efficient pseudopotentials for plane-wave calculations. *Phys. Rev. B* **1991**, *43*, 1993–2006.
- (62) Hirshfeld, F. L. Bonded-atom fragments for describing molecular charge densities. *Theoret. Chim. Acta* **1977**, *44*, 129–138.
- (63) Cai, Z.-L.; Sendt, K.; Reimers, J. R. Failure of density-functional theory and time-dependent density-functional theory for large extended pi systems. *J. Chem. Phys.* **2002**, *117*, 5543–5549.
- (64) Gritsenko, O.; Baerends, E. J. Asymptotic correction of the exchange–correlation kernel of time-dependent density functional theory for long-range charge-transfer excitations. *J. Chem. Phys.* **2004**, *121*, 655–660.
- (65) Cohen, A. J.; Mori-Sánchez, P.; Yang, W. Challenges for Density Functional Theory. *Chem. Rev.* **2011**, *112*, 289–320.
- (66) Laasonen, K.; Sprik, M.; Parrinello, M.; Car, R. “Ab initio” liquid water. *J. Chem. Phys.* **1993**, *99*, 9080–9089.